Journal of Applied Polymer Science

Functionalization and Hemocompatibility of a Styrenic Thermoplastic Elastomer Based on Its Epoxidized Precursor

Shuaishuai Yuan,[1,2] Shifang Luan,[1] Huawei Yang,[1] Hengchong Shi,[1] Jing Jin,[1] Lingjie Song,[1,2] Jiao Ma,[1] Jinghua Yin[1]

[1]State Key Laboratory of Polymer Physics and Chemistry, Changchun Institute of Applied Chemistry, Chinese Academy of Sciences, Changchun 130022, China

[2]University of Chinese Academy of Sciences, Beijing 100049, China

Correspondence to: S. Luan (E-mail: sfluan@ciac.ac.cn) or J. Yin (E-mail: yinjh@ciac.ac.cn)

ABSTRACT: Poly(ethylene glycol) monomethyl ether (mPEG) was introduced into a glycidyl methacrylate-modified styrenic thermoplastic elastomer graft copolymer via a ring-opening reaction with the epoxy group. The chemical compositions of the samples were confirmed by Fourier transform infrared spectroscopy, ^{1}H-NMR spectroscopy, and gel permeation chromatography. X-ray photoelectron spectroscopy, atomic force microscopy, and water contact angle measurement were used to investigate the surface properties. The results show that the molecular weight of the mPEG monomer had a great effect on the surface properties of the modified samples. The platelet adhesion and protein adsorption of the samples modified with low-molecular-weight mPEG were reduced dramatically relative to those of the virgin styrenic thermoplastic elastomer. © 2014 Wiley Periodicals, Inc. J. Appl. Polym. Sci. **2014**, *131*, 40518.

KEYWORDS: biocompatibility; biomedical applications; grafting; polyolefins

Received 1 October 2013; accepted 27 January 2014
DOI: 10.1002/app.40518

INTRODUCTION

Because of its excellent clarity, good thermal stability, outstanding mechanical performance, and radiation sterilization, styrenic thermoplastic elastomers (TPSs) are used to fabricate medical devices, such as catheters, transfusion bags, heart valves, substrates for cell cultures, and stent drug-delivery coatings.[1–4] TPSs derive excellent properties from their ability to form styrene (hard-phase) and olefin (rubber-phase) domains with well-defined morphologies. However, the inertness and hydrophobic properties of their polyolefin backbone has limited the use of TPSs in applications that require, for example, blood-compatible surfaces.[5] When blood makes contact with the hydrophobic surface of polymers, the surface tends to adsorb plasma protein at the initial stage; this is followed by platelet adhesion and their activation and eventually clot or thrombus formation.[6]

To improve the surface blood compatibility of a substrate, two main methods have been reported: surface modification and bulk modification. Surface functionalization is an efficient techniques for improving the surface performance of existing polymers without great changes to their bulk properties. Various hemocompatible moieties have been used for surface modification;[7] these have included poly(ethylene glycol) (PEG) and its derivatives,[8–16] poly(vinyl pyrrolidone),[17–22] zwitterionic materials,[23–27] heparin,[28,29] chitosan,[20–33] proteins,[34–36] and lysine.[37] Furthermore, bulk modification is another method for obtaining biocompatible surfaces. Generally, there are three contemporary methodologies that are used for bulk modification: physical blending,[38] copolymerization,[39] and chemical grafting.[40] The surface properties of the functionalized polymers via bulk modification can still be maintained even after further processing. For practical and economic considerations, melt grafting based on free-radical polymerization is a particularly attractive method among bulk modifications.[41,42] However, the high temperature during the process can result in a low grafting degree (GD) of the monomer and even severe crosslinking or degradation.

To enhance the GD or reduce side reactions, various reagents have been used as coagents during melt-phase processing.[43] It was found that styrene can increase the GD of glycidyl methacrylate (GMA) better than single-monomer grafting. The mechanism of the high GD was ascribed to styryl radicals, and GMA can react with styryl radicals to form polymer-*g*-(GMA-*co*-Styrene (St)).[44,45] Previously, we reported that *N*-vinyl pyrrolidone (NVP) is an efficient promoter for the grafting of GMA onto the TPS backbone, and the maximum GD and grafting efficiency we attained were 2.6 wt % and 87%, respectively. The GDs were increased 7.5- and 2.5-fold compared to those of

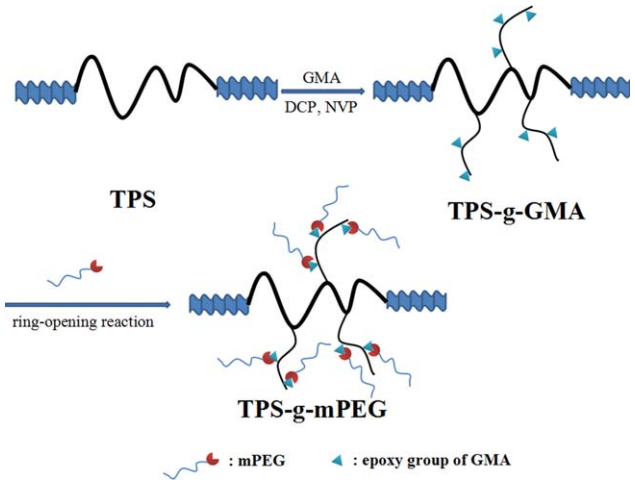

Scheme 1. Synthesis of TPS-*g*-mPEG via a ring-opening reaction. [Color figure can be viewed in the online issue, which is available at wileyonlinelibrary.com.]

single GMA and styrene-assisted grafting, respectively.[46] It is known that GMA-functionalized copolymers can react further with carboxyl, hydroxyl, and amine groups. Many researchers have reported the use of GMA-grafted copolymers as a compatibilizer in polyester blends through the reaction between GMA and the hydroxyl/carboxyl end groups of polyesters.[47,48] The functionalization of GMA-grafted copolymers is an attractive method for expanding their application. PEG and its derivatives were selected for their wide use in materials science and biotechnology because of their low toxicity and good biocompatibility. These materials can prevent protein absorption and cellular adhesion because of their low polymer–water interfacial energy.[49] Wesslen and Wesslen[50] found that a water-soluble polymer could be obtained through the grafting of poly(ethylene glycol) monomethyl ethers (mPEG) onto GMA copolymers.

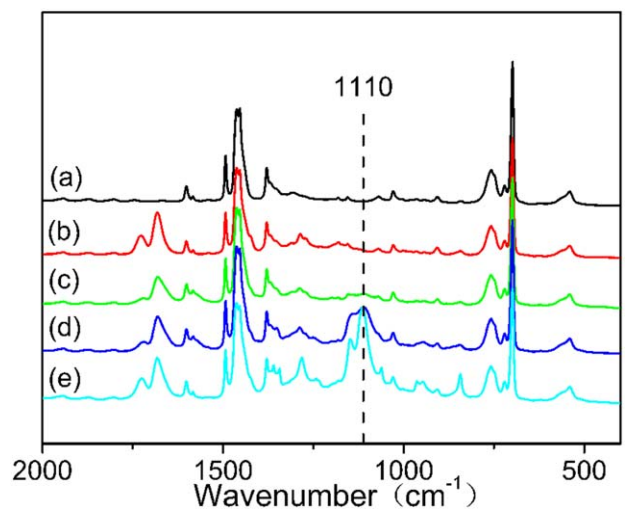

Figure 1. Normalized FTIR spectra of (a) TPS, (b) TPS-*g*-GMA, (c) TPS-*g*-mPEG$_{350}$, (d) TPS-*g*-mPEG$_{1000}$, and (e) TPS-*g*-mPEG$_{5000}$. [Color figure can be viewed in the online issue, which is available at wileyonlinelibrary.com.]

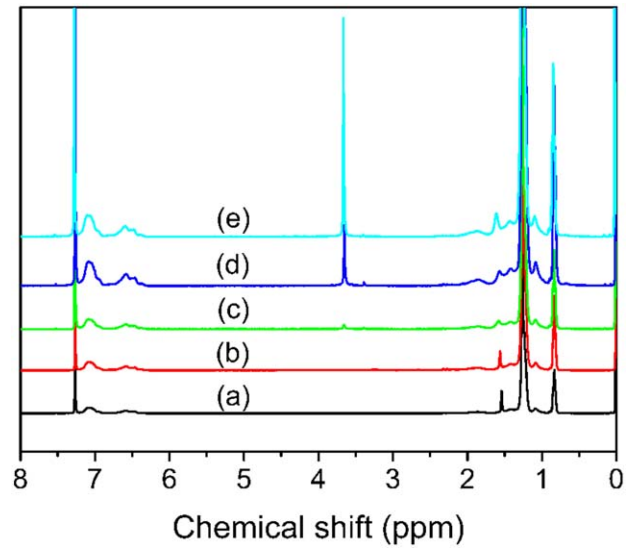

Figure 2. ^{1}H-NMR spectra (400 MHz) of (a) TPS, (b) TPS-*g*-GMA, (c) TPS-*g*-mPEG$_{350}$, (d) TPS-*g*-mPEG$_{1000}$, and (e) TPS-*g*-mPEG$_{5000}$. [Color figure can be viewed in the online issue, which is available at wileyonlinelibrary.com.]

After the reaction, no epoxy groups were found in the soluble graft copolymer without crosslinking.

In this study, mPEG was covalently immobilized onto a GMA-modified copolymer (TPS-*g*-GMA) on the basis of an NVP-assisted grafting procedure by means of a ring-opening reaction with the epoxy group; this rendered the TPS graft copolymer hemocompatible. The mPEG-grafted copolymers were characterized by Fourier transform infrared (FTIR) spectroscopy, ^{1}H-NMR spectroscopy, gel permeation chromatography (GPC), and differential scanning calorimetry (DSC). Their surface properties were studied by atomic force microscopy (AFM), water contact angle (WCA) measurement, X-ray photoelectron spectroscopy

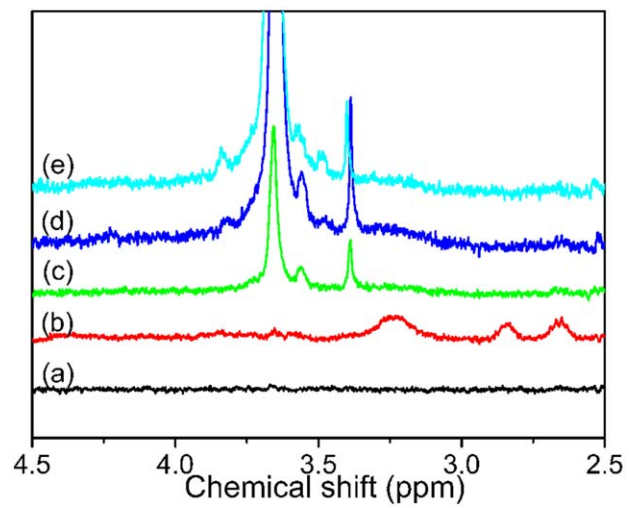

Figure 3. ^{1}H-NMR spectra (enlarged) of (a) TPS, (b) TPS-*g*-GMA, (c) TPS-*g*-mPEG$_{350}$, (d) TPS-*g*-mPEG$_{1000}$, and (e) TPS-*g*-mPEG$_{5000}$. [Color figure can be viewed in the online issue, which is available at wileyonlinelibrary.com.]

Table I. Molecular Weights and Surface Energies of the TPS Samples

Sample	M_w (g/mol)	M_n (g/mol)	M_w/M_n	Surface energy (mJ/m^2)	GD_{mPEG} (wt %)
TPS	107,049	96,892	1.10	17.1	—
TPS-*g*-GMA	108,358	93,660	1.16	15.0	—
TPS-*g*-mPEG$_{350}$	107,268	89,679	1.20	43.1	1.3
TPS-*g*-mPEG$_{1000}$	105,547	87,900	1.20	34.1	3.4
TPS-*g*-mPEG$_{5000}$	106,971	91,430	1.17	29.4	9.7

M_w, weight-average molecular weight.

(XPS), and a biological assay of protein adsorption and platelet adhesion.

EXPERIMENTAL

Materials

A TPS copolymer with 29 wt % styrene (Kraton G 1652) was purchased from Shell Chemical Co., Ltd. mPEGs with number-average molecular weights (M_ns) of 5000, 1000, and 350 were used as received (Aldrich). Sodium methoxide was purchased from J&K Scientific, Ltd. (China). NVP was supplied by Shanghai Bangcheng Chemical Co., Ltd. GMA was obtained from Shanghai Nuotai Chemical Co., Ltd. (China). Dicumyl peroxide was purchased from Beijing Chemical Factory (China). Bovine serum albumin (BSA) and sodium dodecyl sulfate (SDS) were obtained from Dingguo Bio-Technology (China). Freshly prepared phosphate-buffered saline (PBS; 0.1 mol/L, pH = 7.4) was used for protein adsorption and platelet adhesion. A Micro bicinchoninic acid protein assay reagent kit was obtained from Boster Biological Technology (AR1100, China). The other reagents were analytical reagent grade, and all of the materials were used as received directly without further purification.

Sample Preparation

The TPS copolymer (35.00 g), dicumyl peroxide (0.14 g), NVP (1.75 g), and GMA (1.05 g) were premixed, and then, the grafting reactions were carried out in a Haake internal mixer at a desired temperature with a screw speed of 60 rpm, as previously reported.[46] After 5 min of grafting reaction, the products were removed from the chamber and cooled at room temperature. The grafted TPS (denoted as TPS-*g*-GMA) was dissolved in xylene at room temperature for 24 h, precipitated by an ethanol/acetone mixture (volume ratio = 1/4), washed, filtered, and finally dried in a vacuum oven at 40°C for 48 h.

The TPS-*g*-GMA was dissolved in toluene and dried by azeotropic distillation. mPEG was dried similarly, and then, a suitable amount of sodium methoxide was added to the mPEG solution. The mixture was refluxed, and the formed methanol was distilled off with toluene. The solutions of TPS-*g*-GMA and mPEG–alkoxide were mixed and refluxed for 2 h under N_2. Then, the resulting products [denoted as TPS-*g*-mPEG$_N$ (where *N* denotes molecular weight of mPEG)] were precipitated by an ethanol/acetone mixture. After the evaporation of the solvent, the products were then dried to a constant weight in a vacuum oven at 40°C for 48 h.

Characterization

TPS, TPS-*g*-GMA, and TPS-*g*-mPEG$_N$ were hot-compressed into a film at 130°C. The IR spectra of them were then tested by a Bruker Vertex 70 FTIR spectrometer.

The ^{1}H-NMR spectra were collected on a Bruker AV 400 M NMR spectrometer with deuterated chloroform as the solvent and tetramethylsilane (chemical shift in nuclear magnetic resonance (NMR) spectroscopy (δ) = 0) as the internal standard at room temperature.

The molecular weight and molecular weight distribution of the sample was determined at 150°C by a PL-GPC220 type high-temperature chromatograph equipped with three PL gel 10-μm mixed-B light scattering (LS) type columns. 1,2,4-Trichlorobenzene was used as the eluent at a flow rate of 1.0 mL/min.

The melting and crystallization behaviors of the samples were determined on a PE DSC-7. Samples of about 5 mg were annealed at 150°C for 3 min to erase the thermal history. Then, the samples were cooled to −50°C at a rate of 10°C/min and subsequently heated to 150°C at a rate of 10°C/min. The curves

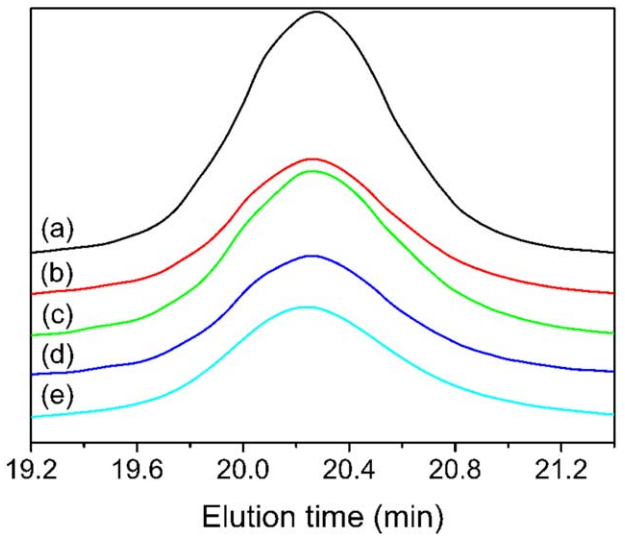

Figure 4. GPC elution curves of the samples: (a) TPS, (b) TPS-*g*-GMA, (c) TPS-*g*-mPEG$_{350}$, (d) TPS-*g*-mPEG$_{1000}$, and (e) TPS-*g*-mPEG$_{5000}$. [Color figure can be viewed in the online issue, which is available at wileyonlinelibrary.com.]

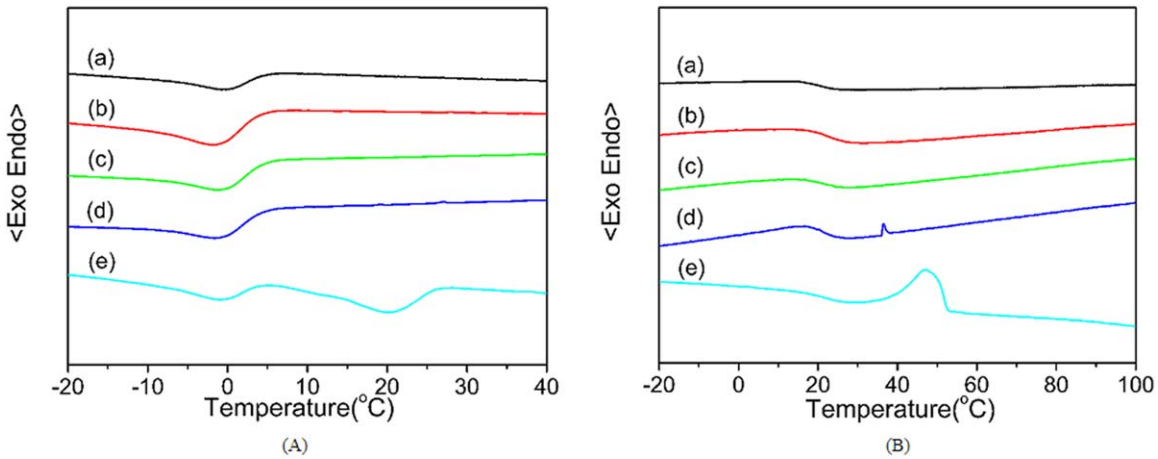

Figure 5. (A) DSC cooling curves and (B) heating curves of (a) TPS, (b) TPS-*g*-GMA, (c) TPS-*g*-mPEG$_{350}$, (d) TPS-*g*-mPEG$_{1000}$, and (e) TPS-*g*-mPEG$_{5000}$. [Color figure can be viewed in the online issue, which is available at wileyonlinelibrary.com.]

were recorded, and the corresponding temperature (T_c) and melting temperature (T_m) were determined.

Surface Performance

The films were prepared by the casting of 10% w/v solutions of the TPS, TPS-*g*-GMA, and TPS-*g*-mPEG$_N$ in chloroform onto clean glass slides in Petri dishes for 12 h at room temperature. The as-prepared films were then dried *in vacuo* for 12 h at room temperature to completely remove the solvent.

The surface morphology was examined with AFM in contact mode (SPA300HV with an SPI 3800 controller, Seiko Instruments Industry, Japan). The root mean square roughness (RMS) was evaluated from the AFM images.

The WCAs of the TPS, TPS-*g*-GMA, and TPS-*g*-mPEG$_N$ membranes were recorded with a drop-shape analysis instrument (Krüss Gmbh). A 2-mL droplet of water was initially deposited onto the member surface. The contact angle values used were an average of five measurements on different areas of each sample.

Equation of state theory (Neumann) is a universal method for calculating the surface free energy of polymers with the contact angle value. The Neumann method is a transformation of Young's equation; it combines the basic assumption that the surface energy of a solid–liquid interface (γ_{sl}) depends on the properties of the solid and measuring liquid:

Young's equation:

$$\gamma_{sl}=\gamma_s-\gamma_l\cos\theta$$

Equation of state:

$$\gamma_{sl}=f(\gamma_s,\gamma_l)$$

$$\gamma_{sl}=\gamma_s+\gamma_l-2(\gamma_s\gamma_l)^{0.5}\exp\{-\beta_1(\gamma_l-\gamma_s)^2\}$$

Neumann equation:

$$(\gamma_s/\gamma_l)^{0.5}\exp\{-\beta_1(\gamma_l-\gamma_s)^2\}=0.5(1+\cos\theta)$$

where γ_s and γ_l represent the solid and liquid surface energy, respectively, and θ is the contact angle between the solid and liquid. The coefficient $\beta_1 = 0.0001247$ was determined experimentally.

The surface elemental compositions of the TPS films were examined by XPS (VG Scientific ESCA MK II Thermo Advantage V 3.20 analyzer) with an Al/K (photons energy (h_v) = 1486.6 eV) anode mono-X-ray source at a detection angle of 90°. The spectra were collected over the range 0–1200 eV, and high-resolution spectra of the C_{1s}, N_{1s}, and O_{1s} regions were provided. The atomic concentrations of the elements were determined by the peak area ratios.

Table II. DSC Data for the Samples

Sample	T_{c1} (°C)	ΔH_m (J/g)	T_{c2} (°C)	ΔH_m (J/g)	T_{m1} (°C)	ΔH_c (J/g)	T_{m2} (°C)	ΔH_c (J/g)
TPS	−0.7	7.4	—	—	14.4	10.3	—	—
TPS-*g*-GMA	−1.9	8.6	—	—	12.9	7.3	—	—
mPEG$_{350}$	—	—	−20.3	88.7	—	—	−0.5	56.1
TPS-*g*-mPEG$_{350}$	−1.2	9.3	—	—	10.0	7.6	—	—
mPEG$_{1000}$	—	—	28.6	161.6	—	—	43.2	166.6
TPS-*g*-mPEG$_{1000}$	−1.5	9.0	—	—	14.4	9.1	36.5	0.6
mPEG$_{5000}$	—	—	39.1	182.2	—	—	65.2	186.8
TPS-*g*-mPEG$_{5000}$	−1.0	7.5	20.1	9.9	15.0	6.4	47.2	9.5

ΔH_m is melting enthalpy.
ΔH_c is crystallization enthalpy.

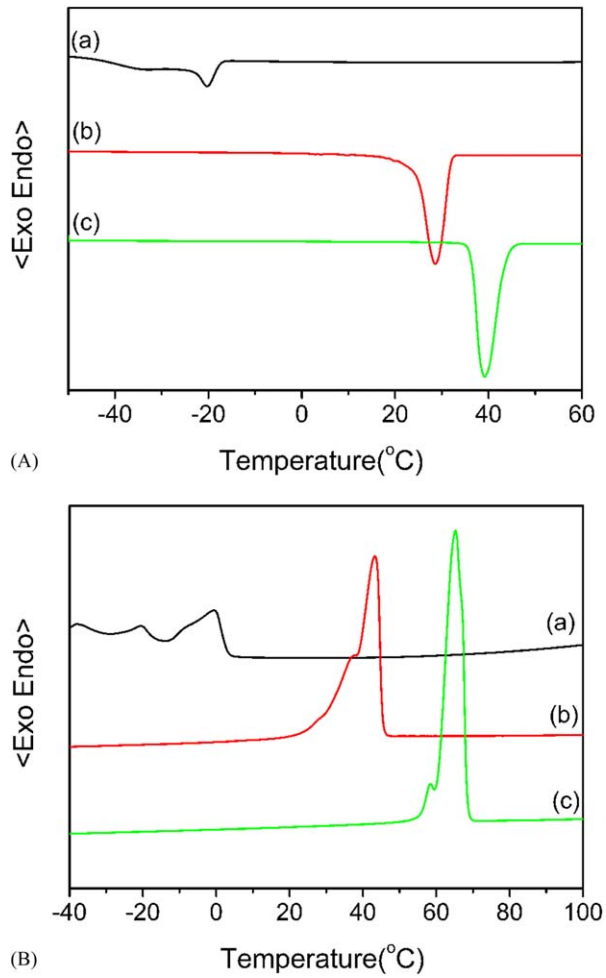

Figure 6. (A) DSC cooling curves and (B) heating curves of (a) $mPEG_{350}$, (b) $mPEG_{1000}$, and (c) $mPEG_{5000}$. [Color figure can be viewed in the online issue, which is available at wileyonlinelibrary.com.]

The surface atomic concentrations (*Cs*) of the elements were determined by the peak area ratios. The N/C ratio was obtained directly from the surface atomic concentrations of N and C. The C_{C-O}/C ratios were calculated from the following equation after nonlinear Gaussian fitting of the C_{1s} spectra:

$$\frac{C_{C-O}}{C} = \left(\frac{A_{C286.0}}{A_{Ctotal}} - \frac{N}{C}\right) \times 100\%$$

where $A_{C286.0}$ is the peak area corresponding to C_{C-O} and C_{C-N} after the fitting of the C_{1s} spectrum and A_{Ctotal} is the total peak area of the C_{1s} spectrum.

Protein Adsorption

The TPS and TPS-*g*-$mPEG_N$ films were immersed in PBS (pH 7.4) for at least 12 h to equilibrate the surfaces. Then, the films were dipped into a PBS solution containing BSA (1.0 mg/mL) for 2 h at 37°C. After several rinsings with fresh PBS, the samples were immersed in an aqueous solution of 1.0 wt % SDS and subjected to shaking for 60 min at room temperature to remove the proteins adsorbed on the surfaces. The protein concentration in the SDS solution, on the basis of the bicinchoninic acid protein assay kit method, was determined with a microplate reader (Tecan Sunrise, Switzerland), and the amount of proteins adsorbed on the surfaces was calculated.

Platelet Adhesion

The films were incubated in a tissue culture plate with PBS for 2 h. Fresh blood collected from a healthy rabbit was immediately mixed with a 3.8 wt % sodium citrate solution at a dilution ratio of 9:1. The platelet-rich plasma was obtained from the fresh rabbit blood by centrifugation at 800 rpm for 10 min. Then, fresh platelet-rich plasma (20 μL) was dropped onto each film and incubated for 60 min at 37°C. After they were washed with PBS, the adhered platelets on the films were fixed by 2.5 wt % glutaraldehyde for more than 10 h at 4°C. Finally, the films were washed with PBS several times and dehydrated with a series of ethanol/water mixtures (30, 50, 70, 90, and 100 vol % ethanol). The samples were observed with field emission scanning electron microscopy (SEM; XL 30 ESEM FEG, FEI Co.). The number of adhered platelets on the films was calculated from several SEM pictures of the same films at a magnification of about 2000×.

RESULTS AND DISCUSSION

Characterization of the Samples

Scheme 1 depicts the covalent immobilization of mPEG onto TPS. Step 1 involved the formation of epoxy groups on TPS via the NVP-assisted melt grafting of GMA in a Haake internal mixer. In step 2, mPEG was coupled to the epoxy group of TPS-*g*-GMA by a ring-opening reaction.

The samples were examined by IR spectroscopy as described in the Experimental section. As shown in Figure 1, all of the spectra were normalized by the peak area at 1500 cm^{-1}, which was assigned to the —C=C— stretching of PS. The strongest absorption peaks at 1378 and 1461 cm^{-1} were assigned to the C—H bending vibrations of the CH_3 and CH_2 groups of the ethylene and butylene block in SEBS (EB) block, respectively.[51] The two bands observed at 700 and 762 cm^{-1} were representative of the =C—H bending vibrations associated with the phenyl group in the styrene block. The absorption peak of —C—O— at about 1110 cm^{-1} (the ester bond in mPEG) verified the occurrence of the grafting reaction of mPEG. In contrast, the spectra of TPS-*g*-$mPEG_{350}$, TPS-*g*-$mPEG_{1000}$, and TPS-*g*-$mPEG_{5000}$ at 1110 cm^{-1} [Figure 1(c–e)] demonstrated that the GD of mPEG was obviously enhanced with the increase of the molecular weight.

Samples c, d, and e presented additional peaks at 3.6 and 3.4 ppm; these were attributed to the protons of mPEG in ^{1}H-NMR curves (Figures 2 and 3). With increasing mPEG molecular weight, the relative intensities of the peak at 3.6 ppm gradually increased. The GDs of mPEG were calculated from ^{1}H-NMR spectroscopy and are shown in Table I. When the molecular weight increased, the GD increased from 1.3 wt % (TPS-*g*-$mPEG_{350}$) to 9.7 wt % (TPS-*g*-$mPEG_{5000}$).

The GDs of mPEG in these materials were determined by ^{1}H-NMR from the following equation:

$$GD_{mPEG} = \frac{A_{3.6} \times M_{mPEG} \times 5 \times 0.29}{A_{Ph} \times 104 \times (4n-2)} \times 100\%$$

where $A_{3.6}$ denotes the sum of the areas under the peaks corresponding to the methylene protons in the mPEG, A_{Ph} denotes the sum of areas under the peaks corresponding to the

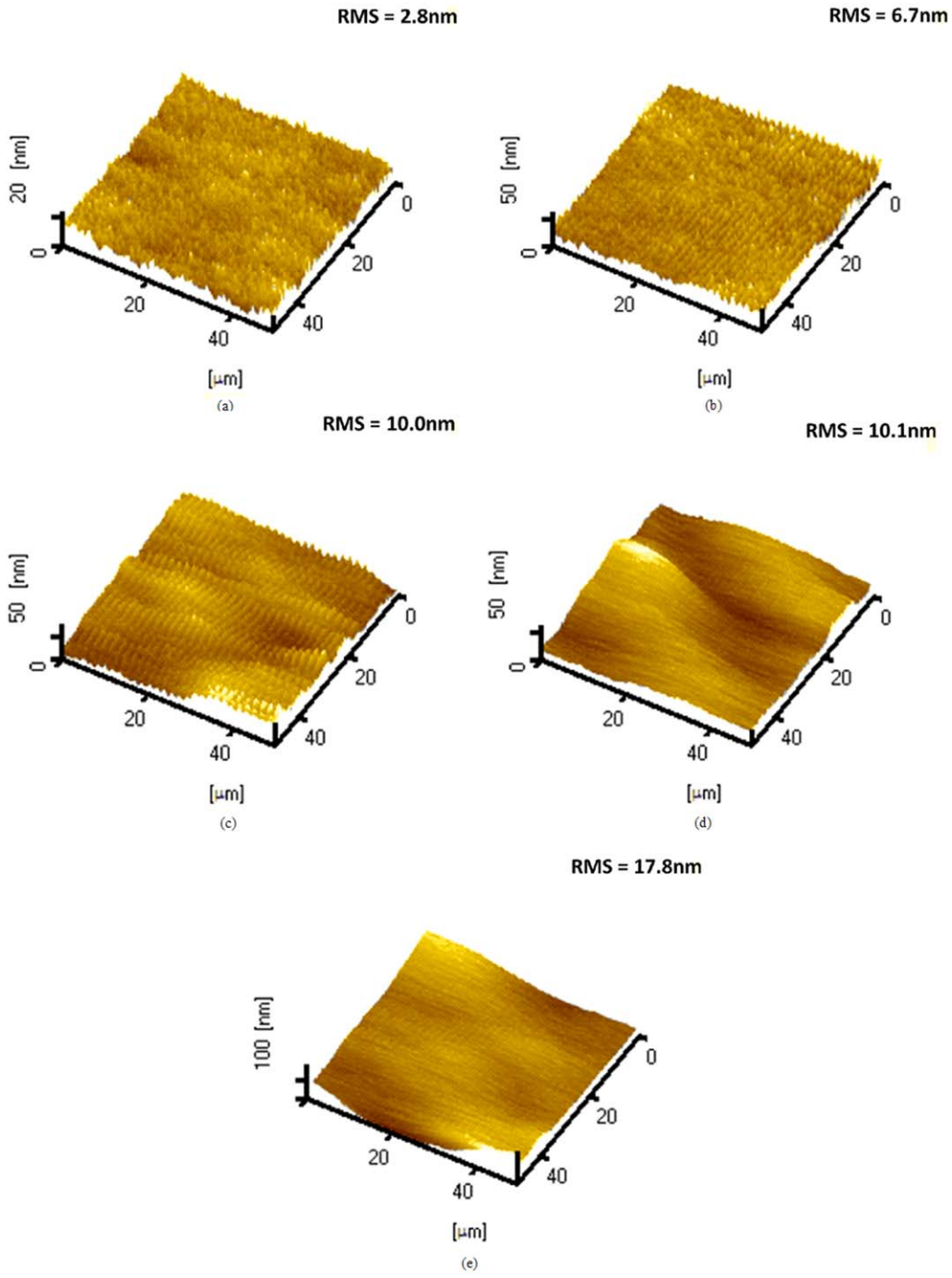

Figure 7. AFM images of (a) TPS, (b) TPS-*g*-GMA, (c) TPS-*g*-mPEG$_{350}$, (d) TPS-*g*-mPEG$_{1000}$, and (e) TPS-*g*-mPEG$_{5000}$. [Color figure can be viewed in the online issue, which is available at wileyonlinelibrary.com.]

TPS–phenyl protons (6.3–7.2 ppm), 0.29 denotes the weight percentage of the PS block in TPS, 104 is the molecular weight of styrene, M_{mPEG} denotes the average molecular weight of the mPEG monomer, and n denotes the number of ethylene glycol repeating units in the mPEG. The molecular weights of the samples changed slightly after the reactions (Figure 4 and Table I); this suggested no apparent degradation or crosslinking, which absolutely meets the requirements of practical applications.

Thermal Behaviors of the Samples

It was of great interest to investigate the effect of mPEG on the crystallization and melting behavior of TPS after modification. To determine the effect of mPEG incorporation, all of samples were analyzed with DSC according to the conditions described in the Characterization section. The nonisothermal crystallization curves of the TPS and mPEG-functionalized TPS during the cooling process are shown in Figure 5(A), and the corresponding data are illustrated in Table II. We observed that the

Table III. Atomic Concentrations of the TPS and mPEG-Modified TPS

	Atomic concentration (%)				
Sample	C_{1s}	O_{1s}	N_{1s}	C_{C-O}/C	Theoretical C_{C-O}/C
TPS	91.07	8.93	0	0	0
TPS-*g*-mPEG$_{350}$	81.09	17.44	1.48	15.95	0.79
TPS-*g*-mPEG$_{1000}$	82.26	16.66	1.08	15.96	2.04
TPS-*g*-mPEG$_{5000}$	87.15	12.4	0.45	7.70	5.62

crystallization temperatures of the mPEG-functionalized TPS samples were lower than those of the virgin TPS; this indicated that mPEG disordered the crystallization of TPS. Figure 6(A) shows the nonisothermal crystallization curves of mPEG$_{350}$, mPEG$_{1000}$, and mPEG$_{5000}$. It was clear that the TPS disordered the crystallization of mPEG (Table II). The virgin TPS showed one peak at −0.7°C, which was due to the crystallization of —$(CH_2—CH_2)_n$ in the PEB block. Also, there was only one peak in the samples of TPS-*g*-mPEG$_{350}$ and TPS-*g*-mPEG$_{1000}$, whereas TPS-*g*-mPEG$_{5000}$ had two peaks at −1.0 and 20.1°C, and the appearance of a new peak at 20.1°C was attributed to mPEG.

The T_m of the mPEG-functionalized TPS samples increased with increasing molecular weight of mPEG [Figure 5(B) and Table II]. The melting points of mPEG were −20.3°C (mPEG$_{350}$), 43.2°C (mPEG$_{1000}$), and 65.2°C (mPEG$_{5000}$), respectively [Figure 6(B) and Table II]. Similar to the behavior that Ganguly, A reported,[52] the melting curve of TPS provided one major melting peak at 14.4°C, and the TPS-*g*-mPEG$_{350}$ presented one

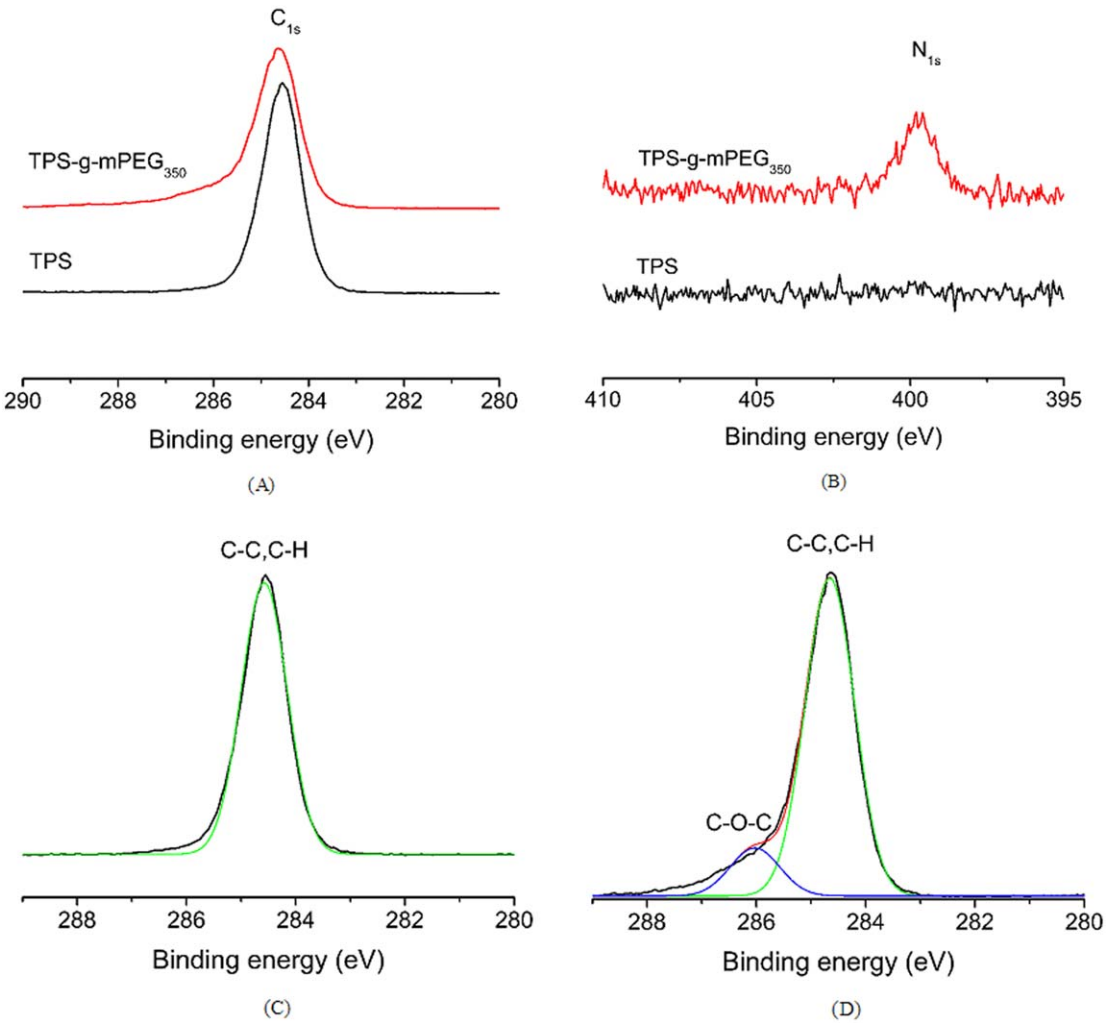

Figure 8. XPS spectra of (A) C_{1s} and (B) N_{1s} of TPS and TPS-*g*-mPEG$_{350}$ and high-resolution C_{1s} fitting curves of (C) TPS and (D) TPS-*g*-mPEG$_{350}$. [Color figure can be viewed in the online issue, which is available at wileyonlinelibrary.com.]

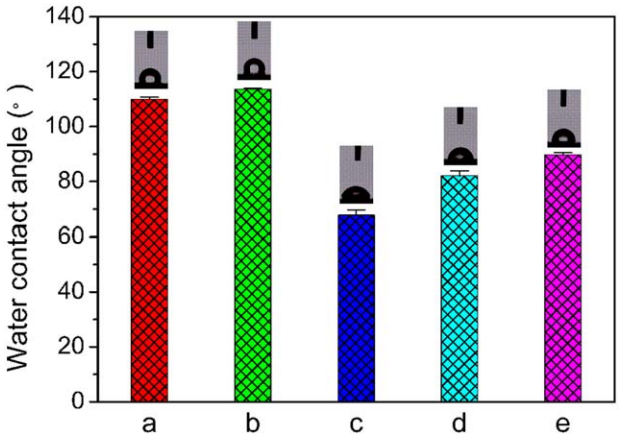

Figure 9. WCAs of the samples: (a) TPS, (b) TPS-*g*-GMA, (c) TPS-*g*-mPEG$_{350}$, (d) TPS-*g*-mPEG$_{1000}$, and (e) TPS-*g*-mPEG$_{5000}$. [Color figure can be viewed in the online issue, which is available at wileyonlinelibrary.com.]

melting peak at 10.0°C. In particular, TPS-*g*-mPEG$_{1000}$ and TPS-*g*-mPEG$_{5000}$ exhibited additional melting peaks at 36.5 and 47.2°C, respectively; this was attributed to the melting of mPEG.

The GDs of mPEG had a great effect on the crystallization and melting behaviors of mPEG-modified TPS. The TPS-*g*-mPEG$_{350}$ had a slight effect on the PEB block in TPS, whereas the TPS-*g*-mPEG$_{1000}$ and TPS-*g*-mPEG$_{5000}$ changed the crystallization and melting behaviors of TPS.

Surface Morphology, Composition, and Wettability

Figure 7 shows the AFM surface topography of the TPS samples. The virgin TPS illustrated a rough surface with an RMS value of about 2.8 nm over the 50 × 50 μm^2 scanning area [Figure 7(a)]. TPS-*g*-GMA showed an increase in the surface roughness (6.7 nm). After the grafting of mPEG, the surface roughness values of TPS-*g*-mPEG$_{350}$, TPS-*g*-mPEG$_{1000}$, and TPS-*g*-mPEG$_{5000}$ increased further to 10.0, 10.1, and 17.8 nm, respectively.

The surface chemical composition of the TPS samples was characterized with XPS measurement, and the results are listed in Table III. A large amount of oxygen was detected in both the virgin and modified samples. The phenomena was reported by our group and another research group that the oxygen contamination of the TPS surface was hardly prevented.[42,46,53] After the introduction of mPEG, the oxygen content of the samples increased from 8.93 to 17.44% (TPS-*g*-mPEG$_{350}$), 16.66% (TPS-*g*-mPEG$_{1000}$), and 12.4% (TPS-*g*-mPEG$_{5000}$). Compared to the virgin TPS, a new peak of N_{1s} appeared in the spectrum of TPS-*g*-mPEG$_{350}$; this indicated the presence of a coagent NVP moiety [Figure 8(B)]. The high-resolution C_{1s} spectra of the TPS membrane had only one peak [C—C; Figure 8(C)], whereas that of the TPS-*g*-mPEG$_{350}$ membrane could be resolved into two peaks by a Gaussian peak-fitting algorithm at binding energies of 284.6 eV (C—C peak) and 286.2 eV [C—O—C peak; Figure 8(D)]. As shown in Table III, the C_{C-O}/C ratios of TPS-*g*-mPEG$_{350}$ and TPS-*g*-mPEG$_{1000}$ were higher than that of TPS-*g*-mPEG$_{5000}$. XPS usually provides the statistical atomic composition of the surface and near surface down to a depth of 10 nm. Thus, although TPS-*g*-mPEG$_{350}$ and TPS-*g*-mPEG$_{1000}$ exhibited dissimilar surface performances, their XPS C_{C-O}/C ratios were similar, that is, 15.95 and 15.96%, respectively.

When annealing in the air, low-energy groups (—F, —Si) tend to migrate toward the air/polymer interface, whereas high-energy groups (—OH, —COOH, —NH_2) migrate toward the polymer surface when they are annealed in water vapor.[54] The mPEG-modified TPS samples were dissolved in chloroform, and then cast onto glass in covered Petri dishes. The C_{C-O}/C ratios were calculated after the fitting of the C_{1s} spectra (Table III). Compared with the theoretical values, we found that the chloroform vapor provoked the enrichment of the high-energy mPEG segment onto the polymer surface.

The wettability of the biomedical material surface plays an important role in governing hemocompatibility. Although many factors influence the hemocompatibility of materials, it is believed that a hydrophilic surface can reduce the adsorption of proteins and cells. As shown in Figure 9 and Table I, the virgin TPS surface had an initial WCA of approximately 110°. After the incorporation of GMA, the WCA increased to 113°. The WCAs of the mPEG-modified TPS were lower than that of the virgin TPS. The different molecular weights of the mPEGs showed different WCAs. The WCAs of TPS-*g*-mPEG$_{1000}$ (82°) and TPS-*g*-mPEG$_{5000}$ (89°) changed a little with respect to the that of the virgin TPS. As for TPS-*g*-mPEG$_{350}$, the value decreased to 68°. These results were consistent with our previous report in which low-molecular-weight PEG was prone to moving toward the air interface during film formation because the PEG segment had a higher solubility in chloroform than the poly[styrene-b-(ethylene-co-butylene)-b-styrene] (SEBS) backbone.

Srinivasarao et al.[55] found that the high vapor pressure of the solvent and the velocity of air across the surface drove solvent evaporation and rapidly cooled the surface. They measured this cooling to be as much as 25°C below room temperature; this resulted in an evaporating polymer surface of near 0°C. In

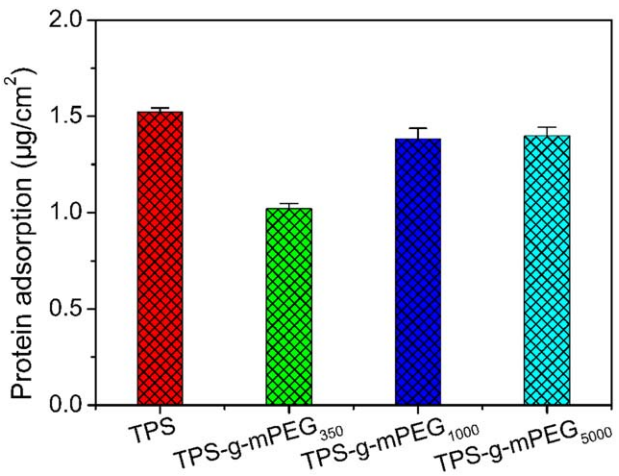

Figure 10. Amount of adsorption of BSA onto the virgin and mPEG–modified TPS. [Color figure can be viewed in the online issue, which is available at wileyonlinelibrary.com.]

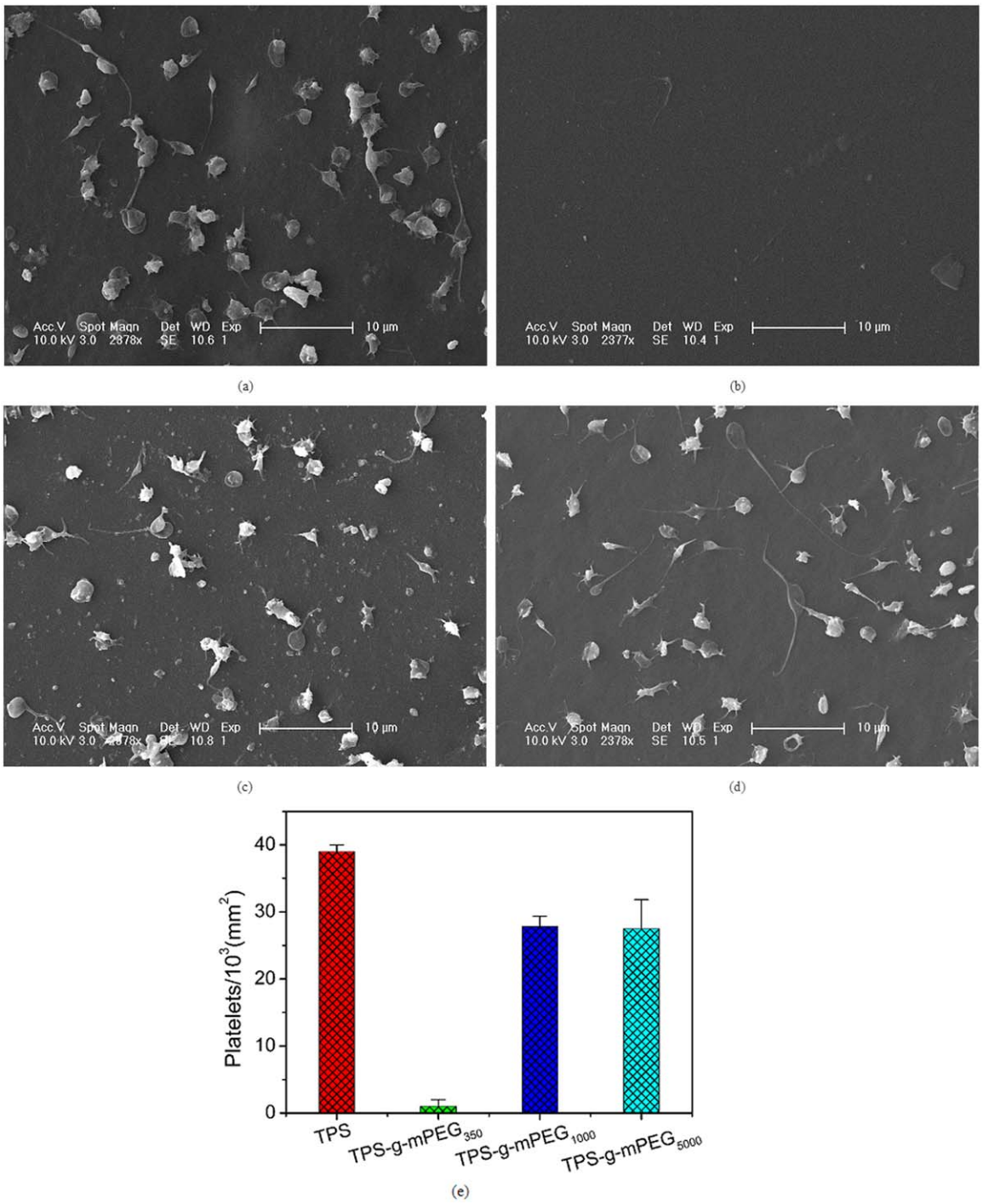

Figure 11. (a–d) SEM images of platelet adhesion on surfaces of TPS, TPS-*g*-mPEG$_{350}$, TPS-*g*-mPEG$_{1000}$, and TPS-*g*-mPEG$_{5000}$, respectively, and (e) statistical number of adherent platelets. [Color figure can be viewed in the online issue, which is available at wileyonlinelibrary.com.]

our experiment, the evaporation of chloroform also led the temperature of the polymer surface to be 0°C. Combining the results of DSC, we concluded that the temperature of the polymer surface during film formation was crucial. The crystallization temperatures of mPEG$_{350}$, mPEG$_{1000}$, and mPEG$_{5000}$ were −20.3, 28.6, and 39.1°C, respectively. During film formation, mPEG$_{1000}$ and mPEG$_{5000}$ were prone to crystallization. This confined the surface enrichment and reorganization of mPEG in the TPS-*g*-mPEG$_{1000}$ and TPS-*g*-mPEG$_{5000}$ films and ultimately affected the wettability of the films. Furthermore, when the environment was changed from a polymer–air interface to a polymer–water interface, the mPEG segment of TPS-*g*-mPEG$_{350}$ was easier to reorganize, whereas the longer backbone and crystallization of mPEG in the TPS-*g*-mPEG$_{1000}$ and TPS-*g*-mPEG$_{5000}$ films both confined the surface enrichment and reorganization of mPEG and, thus, affected the wettability of the

samples. Combining the results of DSC, XPS, and WCA, we concluded that the surface enrichment of mPEG on the surface of TPS-*g*-mPEG$_{350}$ was higher than those of TPS-*g*-mPEG$_{1000}$ and TPS-*g*-mPEG$_{5000}$.

Protein Absorption

The interaction between the protein and polymer surface is critical for many medical applications.[56] Fouling due to protein adsorption is thought to be the key factor in determining subsequent responses, such as platelet adhesion and their activation and blood coagulation. PEG has been widely used for the preparation of antifouling surfaces. Many methods, including the self-assembling of monolayers of alkane thiolate terminated oligo(ethylene glycol)[57] and PEG brushes grafted from a substrate,[11,58] have been used to reach this goal. Although the antifouling mechanism is still unclear, the antifouling surface can be obtained by the immobilization of PEG.

Herein, BSA was used to study the antifouling properties of the virgin and mPEG-modified TPS films as model proteins. It is commonly accepted that the amount of protein adsorbed on virgin TPS is high because of its hydrophobic backbone. The antiprotein adsorption of TPS-*g*-mPEG$_{1000}$ and TPS-*g*-mPEG$_{5000}$ was improved a little, although these samples had a high GD of mPEG, although the amount of adsorbed BSA decreased from 1.5 μg/cm^2 for the virgin TPS substrate to 1.0 μg/cm^2 for the TPS-*g*-mPEG$_{350}$ sample (Figure 10). The improvement in the antifouling of the protein adsorption of TPS-*g*-mPEG$_{350}$ was consistent with the WCA measurement. As for the TPS-*g*-mPEG$_{1000}$ and TPS-*g*-mPEG$_{5000}$ samples, the density of the PEG chain on the surface of these samples was lower than that of TPS-*g*-mPEG$_{350}$ because of the high molecular weight. Both experiment and simulation confirmed that the density of the PEG chain had a bigger effect on antiprotein than the chain length.[59]

Platelet Adhesion

Platelets, anuclear disk cells produced in bone marrow, have a diameter of 3–4 μm. They change in shape with their activation level during activation. There are five morphological change stages of activated platelets: discoid, dendritic, spread-dendritic, spreading, and fully spreading.[60,61] To our knowledge, the platelet adhesion and activation is one of the crucial factors in evaluating the hemocompatibility of materials.

As shown in the morphologies of the platelet of different films in Figure 11, the quantity and morphology of the platelet on the sample were distinct from each other. The statistical number of adherent platelets is shown in Figure 11(e), with numerous platelets distributed on the surface of the virgin TPS [Figure 11(a)] performing as adhesion, spreading, and aggregation. Because of the lower surface free energy, the antiplatelet adhesion properties of TPS-*g*-mPEG$_{1000}$ and TPS-*g*-mPEG$_{5000}$ were nearly unenhanced. However, the TPS-*g*-mPEG$_{350}$ sample had few platelets on the surface. The excellent platelet-repelling ability of TPS-*g*-mPEG$_{350}$ was consistent with the results of WCA and protein adsorption.

CONCLUSIONS

A series of TPS-*g*-mPEG graft copolymers was successfully prepared via the ring-opening reaction with the epoxy group. We found that the molecular weight of mPEG had a great effect on the properties of the modified samples. The low-molecular-weight mPEG (TPS-*g*-mPEG$_{350}$) had a slight effect on the crystallization and melting behaviors of TPS. In comparison with that of virgin TPS, the WCA of TPS-*g*-mPEG$_{350}$ decreased to 68°. Furthermore, the antiplatelet and antifouling properties of TPS-*g*-mPEG$_{350}$ were improved greatly. The GMA-functionalized TPS is expected to be useful in improving the hemocompatibility of TPS via the reaction of GMA and blood-compatibility monomers with carboxyl, hydroxyl, and amine groups.

ACKNOWLEDGMENTS

The authors acknowledge the financial support of the National Science Foundation of China (contract grant numbers 21274150 and 51273200), the Chinese Academy of Sciences Wego Group High-Tech Research & Development Program (2011–2013), and the Scientific Development Program of Jilin Province (contract grant number 20130102064JC).

REFERENCES

1. Pinchuk, L.; Wilson, G. J.; Barry, J. J.; Schoephoerster, R. T.; Pareland, J. M.; Kennedy, J. P. *Biomaterials* **2008**, *29*, 448.
2. Li, X. M.; Luan, S. F.; Shi, H. C.; Yang, H. W.; Song, L. J.; Jin, J.; Yin, J. H.; Stagnaro, P. *Colloid Surf. B* **2013**, *102*, 210.
3. Ranade, S. V.; Richard, R. E.; Helmus, M. N. *Acta Biomater.* **2005**, *1*, 137.
4. Luan, S. F.; Yang, H. W.; Shi, H. C.; Zhao, J.; Wang, J. W.; Yin, J. H. *Nucl. Instrum. Methods Phys. Res. Sect. B* **2011**, *269*, 94.
5. Li, X. M.; Luan, S. F.; Yuan, S. S.; Song, L. J.; Zhao, J.; Ma, J.; Shi, H. C.; Yang, H. W.; Jin, J.; Yin, J. H. *Colloid Surf. B* **2013**,*112*, 146.
6. Spijker, H. T.; Bos, R.; Busscher, H. J.; van Kooten, T. G.; van Oeveren, W. *Biomaterials* **2002**, *23*, 757.
7. Li, D.; Chen, H.; Brash, J. L. *Colloid Surf. B* **2011**, *86*, 1.
8. Zanini, S.; Riccardi, C.; Orlandi, M.; Colombo, C.; Croccolo, F. *Polym. Degrad. Stab.* **2008**, *93*, 1158.
9. Xiu, K. M.; Cai, Q.; Li, J. S.; Yang, X. P.; Yang, W. T.; Xu, F. *J. Colloid Surf. B* **2012**, *90*, 177.
10. Zanini, S.; Orlandi, M.; Colombo, C.; Grimoldi, E.; Riccardi, C. *Eur. Phys. J. D* **2009**, *54*, 159.
11. Li, X. M.; Luan, S. F.; Yang, H. W.; Shi, H. C.; Zhao, J.; Jin, J.; Yin, J. H.; Stagnaro, P. *Appl. Surf. Sci.* **2012**, *258*, 2344.
12. Zanini, S.; Riccardi, C.; Grimoldi, E.; Colombo, C.; Villa, A. M.; Natalello, A.; Gatti-Lafranconi, P.; Lotti, M.; Doglia, S. M. *J Colloid Interface Sci.* **2010**, *341*, 53.
13. Zanini, S.; Muller, M.; Riccardi, C.; Orlandi, M. *Plasma Chem. Plasma Process.* **2007**, *27*, 446.
14. Choi, C. K.; Choi, O.; Jung, D.; Moon, D. W.; Lee, T. G. *Surf. Interface Anal.* **2013**, *45*, 220.
15. Zhang, W.; Lee, H. R. *Surf. Interface Anal.* **2010**, *42*, 1495.
16. Li, D.; Chen, H.; McClung, W. G.; Brash, J. L. *Acta Biomater.* **2009**, *5*, 1864.

17. Edlund, U.; Källrot, M.; Albertsson, A.-C. *J. Am. Chem. Soc.* **2005**, *127*, 8865.
18. Luan, S. F.; Zhao, J.; Yang, H. W.; Shi, H. C.; Jin, J.; Li, X. M.; Liu, J. C.; Wang, J.; Yin, J. H.; Stagnaro, P. *Colloid Surf. B* **2012**, *93*, 127.
19. Nie, S. Q.; Xue, J. M.; Lu, Y.; Liu, Y. Q.; Wang, D. S.; Sun, S. D.; Ran, F.; Zhao, C. S. *Colloid Surf. B* **2012**, *100*, 116.
20. Källrot, M.; Edlund, U.; Albertsson, A. C. *Biomaterials* **2006**, *27*, 1788.
21. Källrot, M.; Edlund, U.; Albertsson, A. C. *Macromol. Biosci.* **2008**, *8*, 645.
22. Källrot, M.; Edlund, U.; Albertsson, A. C. *Biomacromolecules* **2007**, *8*, 2492.
23. Zhao, J.; Shi, Q.; Yin, L. G.; Luan, S. F.; Shi, H. C.; Song, L. J.; Yin, J. H.; Stagnaro, P. *Appl. Surf. Sci.* **2010**, *256*, 7071.
24. Song, L. J.; Zhao, J.; Yang, H. W.; Jin, J.; Li, X. M.; Stagnaro, P.; Yin, J. H. *Appl. Surf. Sci.* **2011**, *258*, 425.
25. Suzuki, H.; Li, L. F.; Nakaji-Hirabayashi, T.; Kitano, H.; Ohno, K.; Matsuoka, K.; Saruwatari, Y. *Colloid Surf. B* **2012**, *94*, 107.
26. Li, Y.; Liu, C. M.; Yang, J. Y.; Gao, Y. H.; Li, X. S.; Que, G. H.; Lu, J. R. *Colloid Surf. B* **2011**, *85*, 125.
27. Byambaa, B.; Konno, T.; Ishihara, K. *Colloid Surf. B* **2012**, *99*, 1.
28. Edlund, U.; Danmark, S.; Albertsson, A. C. *Biomacromolecules* **2008**, *9*, 901.
29. Kuo, Y.-C.; Tsai, Y.-T. *Colloid Surf. B* **2011**, *82*, 616.
30. Wiarachai, O.; Thongchul, N.; Kiatkamjornwong, S.; Hoven, V. P. *Colloid Surf. B* **2012**, *92*, 121.
31. Wang, Y. F.; Hong, Q. F.; Chen, Y. J.; Lian, X. X.; Xiong, Y. F. *Colloid Surf. B* **2012**, *100*, 77.
32. Potarniche, C. G.; Vuluga, Z.; Donescu, D.; Christiansen, J. D.; Eugeniu, V.; Radovici, C.; Serban, S.; Ghiurea, M.; Somoghi, R.; Beckmann, S. *Surf. Interface Anal.* **2012**, *44*, 200.
33. Xin, Z. R.; Hou, J.; Ding, J. T.; Yang, Z. F.; Yan, S. J.; Liu, C. *Appl. Surf. Sci.* **2013**, *279*, 424.
34. Zhu, L. P.; Jiang, J. H.; Zhu, B. K.; Xu, Y. Y. *Colloid Surf. B* **2011**, *86*, 111.
35. Zhang, C.; Jin, J.; Zhao, J.; Jiang, W.; Yin, J. H. *Colloid Surf. B* **2013**, *102*, 45.
36. Shchukarev, A.; Mladenovic, Z.; Ransjo, M. *Surf. Interface Anal.* **2012**, *44*, 919.
37. Li, D.; Chen, H.; Wang, S. S.; Wu, Z. Q.; Brash, J. L. *Acta Biomater.* **2011**, *7*, 954.
38. Seo, J. H.; Matsuno, R.; Konno, T.; Takai, M.; Ishihara, K. *Biomaterials* **2008**, *29*, 1367.
39. Xu, F.; Nacker, J. C.; Crone, W. C.; Masters, K. S. *Biomaterials* **2008**, *29*, 150.
40. Balakrishnan, B.; Kumar, D. S.; Yoshida, Y.; Jayakrishnan, A. *Biomaterials* **2005**, *26*, 3495.
41. Passaglia, E.; Coiai, S.; Augier, S. *Prog. Polym. Sci.* **2009**, *34*, 911.
42. Yang, H. W.; Luan, S. F.; Zhao, J.; Shi, H. C.; Li, X. M.; Song, L. J.; Jin, J.; Shi, Q.; Yin, J. H.; Shi, D. A.; Stagnaro, P. *Polymer* **2012**, *53*, 1675.
43. Moad, G. *Prog. Polym. Sci.* **1999**, *24*, 81.
44. Cartier, H.; Hu, G. H. *J. Polym. Sci. Part A: Polym. Chem.* **1998**, *36*, 1053.
45. Li, J. L.; Xie, X. M. *Polymer* **2012**, *53*, 2197.
46. Yang, H. W.; Luan, S. F.; Zhao, J.; Shi, H. C.; Shi, Q.; Yin, J. H.; Stagnaro, P. *React. Funct. Polym.* **2010**, *70*, 961.
47. Sun, Y. J.; Hu, G. H.; Lambla, M.; Kotlar, H. K. *Polymer* **1996**, *37*, 4119.
48. Hu, G. H.; Sun, Y. J.; Lambla, M. *Polym. Eng. Sci.* **1996**, *36*, 676.
49. Riedel, T.; Riedelova-Reicheltova, Z.; Majek, P.; Rodriguez-Emmenegger, C.; Houska, M.; Dyr, J. E.; Brynda, E. *Langmuir* **2013**, *29*, 3388.
50. Wesslen, B.; Wesslen, K. B. *J. Polym. Sci. Part A: Polym. Chem.* **1989**, *27*, 3915.
51. Zhou, T.; Zhang, A.; Zhao, C. S.; Liang, H. W.; Wu, Z. Y.; Xia, J. K. *Macromolecules* **2007**, *40*, 9009.
52. Ganguly, A.; Bhowmick, A. K.; Li, Y. *J. Macromolecules* **2008**, *41*, 6246.
53. Yadav, S. K.; Mahapatra, S. S.; Cho, J. W.; Lee, J. Y. *J. Phys. Chem. C* **2010**, *114*, 11395.
54. Ruiz, L.; Garay, M. T.; Laza, J. M.; Vilas, J. L.; Rodriguez-Hernandez, J.; Labrugere, C.; Leon, L. M. *Eur. Polym. J.* **2013**, *49*, 130.
55. Srinivasarao, M.; Collings, D.; Philips, A.; Patel, S. *Science* **2001**, *292*, 79.
56. Higgins, M. J.; Molino, P. J.; Yue, Z. L.; Wallace, G. G. *Chem. Mater.* **2012**, *24*, 828.
57. Emmenegger, C. R.; Brynda, E.; Riedel, T.; Sedlakova, Z.; Houska, M.; Alles, A. B. *Langmuir* **2009**, *25*, 6328.
58. Ma, H.; Hyun, J.; Stiller, P.; Chilkoti, A. *Adv. Mater.* **2004**, *16*, 338.
59. Unsworth, L. D.; Sheardown, H.; Brash, J. L. *Langmuir* **2008**, *24*, 1924.
60. Barnhart, M. I.; Walsh, R.; Robinson, J. A. *Ann. N. Y. Acad. Sci.* **1972**, *201*, 360.
61. Goodman, S.; Grasel, T.; Cooper, S.; Albrecht, R. *J. Biomed. Mater. Res.* **1989**, *23*, 105.